PHYSICAL REVIEW B VOLUME 18, NUMBER 10 15 NOVEMBER, 1978

Theoretical study of lithium graphite. I. Band structure, density of states, and Fermi-surface properties

N. A. W. Holzwarth, S. Rabii, and L. A. Girifalco

Departments of Physics, Electrical Engineering and Science, and Metallurgy and Materials Science, and Laboratory for Research on the Structure of Matter, University of Pennsylvania, Philadelphia, Pennsylvania 19104

(Received 8 May 1978)

The results of a detailed band-structure calculation for first-stage lithium graphite (LiC_6) are presented. In addition to the band dispersion, the density of states near the Fermi level, the shape of the Fermi surface, plasma frequencies, optical masses, de Haas–van Alphen frequencies and masses, and interband optical transitions are obtained. It is found that the occupied bands of LiC_6 are essentially those of graphite with A-A layer stacking and 1/6 excess electron per C atom. Except for some hybridization with the Li $2s$ states, the dispersion of the occupied bands in a layer plane is in quantitative agreement with the corresponding dispersion for two-dimensional graphite, as calculated by previous workers. The Fermi level of LiC_6 corresponds to an energy near a saddle point in the π bands of two-dimensional graphite. The Li $2s$ states are found to hybridize with a bonding C π band $\sim$7–9 eV below E_F and to form a metal-like band having a minimum ~ 1.7 eV above E_F. Hybridization of the Li $2s$ states with the Fermi-level bands is weak, so that the metallic properties of LiC_6 are derived from partially filled bands which have primarily C π character. The present results are found to be consistent with experimental measurements of the Fermi-level density of states and of the plasma frequencies.

I. INTRODUCTION

Graphite intercalation compounds have been the subject of several recent experimental and theoretical investigations.[1,2] These highly anisotropic metals are of interest not only because of their unusual electronic and chemical properties, but also because of their technological possibilities.[3] In the present work, we report the results of a detailed band-structure calculation for the compositionally and structurally most simple compound in this class—first-stage lithium-intercalated graphite (LiC_6).[4,5] Although the present work represents the first comprehensive band-structure study of an intercalated graphite compound, extended Hückel calculations for KC_8 have been carried out by Swanson[6] and by Inoshita, Nakao, and Kamimura.[7]

A theoretical idea which has guided much of the research on graphite-intercalation compounds is that it is the π bands of each two-dimensional graphite layer which are being partially filled (in donor compounds) or emptied (in acceptor compounds) in the intercalation process.[8] The focus of the present work is to determine to what extent this two-dimensional rigid-band model is representative of LiC_6 as well as to provide a framework for understanding various experimental results for LiC_6.

Our results are presented in two papers. The outline of paper I is as follows. In Sec. II the crystal structure and effective one-electron potentials for LiC_6 are discussed. In Sec. III the numerical methods used for the band-structure calculations are described. The band structure itself is presented in Sec. IV. An interpolation model for the Fermi-level bands, based on a linear combination of atomic orbitals (LCAO), has been developed in order to evaluate various Fermi-surface properties such as densities of states, de Haas–van Alphen frequencies and masses, and plasma frequencies. These are discussed in Sec. V. Paper I is concluded in Sec. VI with a comparison of the present work with recent experimental results for LiC_6 and other donor intercalates and with the extended Hückel calculations for KC_8.[6,7] Paper II (the following paper[9]) deals with a calculation of the distribution of electronic charge in LiC_6 and a qualitative discussion of its bonding characteristics.

II. CRYSTAL STRUCTURE AND POTENTIAL FOR LiC_6

LiC_6 has the highest symmetry of the graphite intercalation compounds known at the present time—D_{6h}^1.[4,5] Each carbon layer has the two-dimensional hexagonal structure of graphite with a hexagonal lattice constant of $a = 2.485$ Å,[5] a value which is dilated by 1% over that of graphite. The carbon layers are stacked in direct registry with respect to each other, A-A stacking, in contrast to graphite which has an A-B-type stacking. The distance between carbon layers in LiC_6 is $c = 3.706$ Å,[5] a 10% increase over the carbon-layer spacing in graphite. The Li atoms are arranged midway between two carbon layers such that one-third of the C hexagons have Li atoms directly above and below as shown in Fig. 1(a). Figure

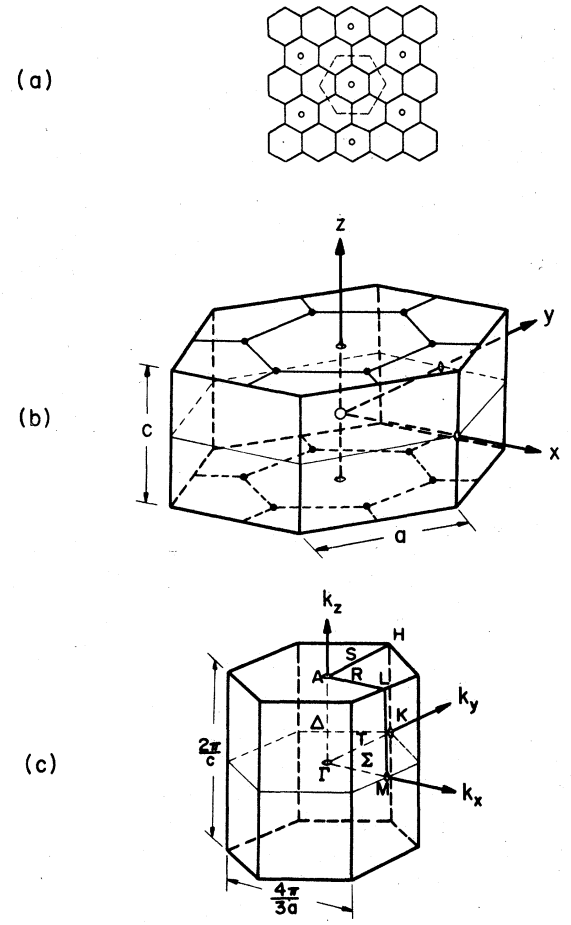

FIG. 1. (a) Projection of c face of LiC_6. Li atoms are denoted by ○, nearest-neighbor C–C bonds are denoted by full lines. The cross section of the unit cell is denoted by a dashed line. (b) Unit cell of LiC_6 showing coordinate system used in present work. The interlayer lattice constant c and the "graphite" interlayer lattice constant a are also noted in the diagram. (The hexagonal intralayer lattice constant of LiC_6 is $\sqrt{3}a$.) (c) Brillouin zone of LiC_6. The special point labels are those of Herring (Ref. 10).

1(b) is a drawing of the three-dimensional unit cell, showing the coordinates used in the present work. Figure 1(c) is a drawing of the corresponding Brillouin zone showing the standard special point labels.[10]

A reasonable approximation to the effective one-electron crystal potential can be obtained from overlapping atomic Coulomb potentials plus an exchange interaction in the Slater $X\alpha$ approximation.[11] For this purpose, it is important to choose the atomic configurations that best approximate the electronic charge density in the crystal. The atomic configuration appropriate for graphite[12] is C $2s^1 2p_{xy}^2 2p_z^1$; the sp_{xy}^2 hybrids form trigonal σ bonds, while the p_z states form the π bands. The suggestion of the idea of "donor" intercalate is that the atoms in LiC_6 have a partial ionic character, Li having positive charge I and C having negative charge $\frac{1}{6}I$, corresponding to the atomic configurations Li $2s^{1-I}$ and C $2s^1 2p_{xy}^2 2p_z^{1+I/6}$, respectively. In the present work, in lieu of a fully self-consistent calculation, band-structure results were obtained for two crystal potentials formed from the two extreme atomic configurations $I=1$ and $I=0$. The ionic potential "$Li^+C_6^-$" ($I=1$) and the neutral potential "LiC_6" ($I=0$) are graphed along various crystal directions in Fig. 2. These were evaluated using atomic charge densities obtained from a Herman-Skillman self-consistent-field program[13] and using the $X\alpha$ exchange parameter 0.77.[14] A further approximation in evaluating these effective one-electron potentials was made in that only spherically symmetric contributions to the charge density of each atom were included. For evaluating the ionic potential ($Li^+C_6^-$), an Ewald summation[15] was used to determine the long-range Coulombic contributions. A summary of lattice constants and potential parameters is given in Table I.

From Fig. 2, it is evident that the ionic potential $Li^+C_6^-$ is generally more repulsive than that of LiC_6, due to the localized repulsive interactions of the $C^{-1/6}$ ions. One expects, and it is verified by the results of the band-structure calculations, that the $Li^+C_6^-$ potential has a stronger attraction toward Li than does the neutral potential. However, this difference in relative potential strength is difficult to see on the scale of Fig. 2, because the Li $2s$ orbital of neutral Li has an extended charge distribution. The striking point illustrated in Fig. 2 is that in both approximations, the crystal potential is found to be highly anisotropic. If one divides the crystal into nonoverlapping muffin-tin spheres, one finds that the anisotropy even within each sphere is far from negligible.

III. NUMERICAL METHODS

Choice of a band-structure-calculation method for LiC_6 requires some care. The extreme anisotropy of the crystal potential mentioned above indicates that band-structure methods based on a muffin-tin-type potential such as Korringa-Kohn-Rostoker (KKR)[16] or augmented-plane-wave (APW)[17] methods would be highly unreliable. The large number of atoms per unit cell (7) would cause a linear-combination-of-atomic-orbitals (LCAO) calculation to be encumbered by a very large number of basis functions per unit cell.[18] The largeness of the unit cell also results in the slow convergence of reciprocal-lattice sums, making orthogonalized-plane-wave[19] or again APW[20] methods inappropriate. Because of these

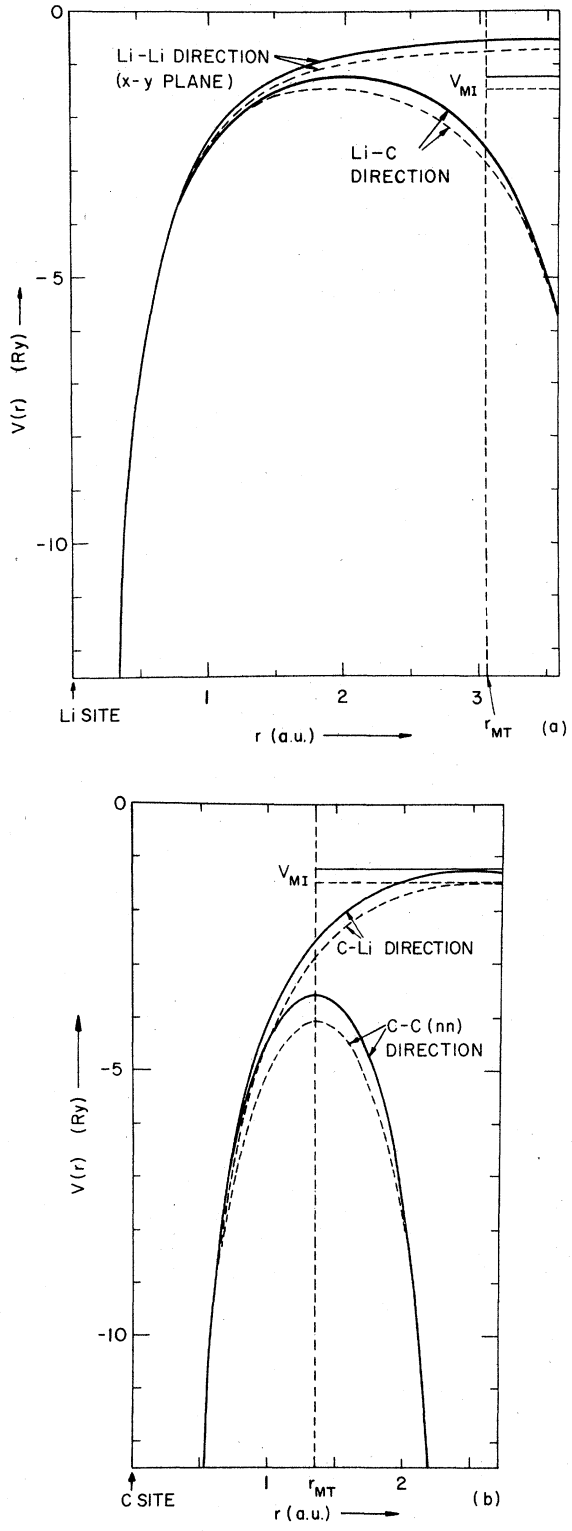

FIG. 2. Effective one-electron crystal potentials near Li (a) and C (b); $Li^+C_6^-$ (full line) and LiC_6 (dashed line) showing also the muffin-tin radii r_{MT}^{Li} and r_{MT}^{C} and the muffin-tin mean interstitial potentials V_{MI}.

TABLE I. Lattice and potential parameters for LiC_6.

Lattice constant parallel to layers (next-nearest C-C distance) (Ref. 5), a	4.6969 a.u.
Lattice constant perpendicular to layers (Ref. 5), c	7.0033 a.u.
Volume of unit cell, Ω	401.3999 a.u.^{3}
Muffin-tin radius of Li, r_{MT}^{Li}	3.0730 a.u.
Muffin-tin radius of C, r_{MT}^{C}	1.3559 a.u.
Ratio of volume inside muffin-tin spheres to total	46%
$X\alpha$ parameter (Ref. 14)	0.77
V_{MI} for $Li^+C_6^-$ potential	−1.23 Ry
V_{MI} for LiC_6 potential	−1.48 Ry

difficulties, one is discouraged from attempting a self-consistent-field calculation for LiC_6. Instead, we chose a band-structure-calculation method which would provide accurate solution of the Schrödinger equation for an electron in either of the two effective crystal potentials described above. By comparing the results from the ionic ($Li^+C_6^-$) and neutral (LiC_6) potentials one can estimate the effects of charge redistribution due to self-consistency on the band structure.

A slightly modified version of the "combined discrete variational method" of Painter[21] was adopted to perform the band-structure calculations in the present work. This method consists of two steps. The first step is a modified KKR[16] calculation to determine the wave functions $\psi_n(\vec{k},\vec{r})$ and energy levels $E_n(\vec{k})$ associated with a muffin-tin form of the crystal potential, $V_{MT}(\vec{r})$. In the present work, $V_{MT}(\vec{r})$ was taken to be the full (not spherically averaged) crystal potential inside the muffin-tin spheres and to be constant, at value V_{MI} equal to the mean interstitial potential, in the interstitial region. The muffin-tin radius of C was chosen to be $\frac{1}{2}$ of the nearest-neighbor C-C separation and the Li sphere was chosen to touch the C sphere. The total sphere volume amounted to 46% of the total crystal volume. The muffin-tin radii r_{MT}^{Li} and r_{MT}^{C} as well as the constant interstitial potentials V_{MI} for $Li^+C_6^-$ and LiC_6 are listed in Table I and are marked on Fig. 2. Scattering by the anisotropic potential within each muffin-tin sphere was taken into account by evaluating the reaction operator K,[22] in the angular-momentum representation. K^{-1} enters the KKR secular equations in the form[23]:

$$\sum_{\sigma' l' m'} \{[K^{\sigma}(E)^{-1}]_{l m, l' m'} \delta_{\sigma\sigma'} + A^{\sigma\sigma'}_{l m, l' m'}(\vec{k},E)\} W^{\sigma'}_{l' m'}(\vec{k},E) = 0 . \quad (1)$$

Here, $A^{\sigma\sigma'}_{lm,l'm'}$ denotes the KKR structure matrix[24] and $W^{\sigma'}_{l'm'}$ denotes a scattered-wave amplitude which enters the evaluation of the muffin-tin wave functions. The summation in Eq. (1) is over all atomic sites σ' within the unit cell and over all angular momenta $l'm'$ for which the scattering is appreciable, i.e., $l' \leq L$, where $|K^{\sigma}_{lm,l'm'}| < \epsilon$ for all $l, l' > L$. In the present work, it was found sufficient to include s- and p-wave scattering only from each of the Li and C sites ($L = 1$) resulting in a KKR secular matrix of dimension 28. Numerical details of the evaluation of the muffin-tin wave functions are presented in the Appendix.

The second step of the band-structure calculation is solution of the Schrödinger equation for the full crystal potential $V(\vec{r})$ using the muffin-tin basis generated in step 1. The final wave function is expressed

$$\Psi_\alpha(\vec{k},\vec{r}) = \sum_n \frac{C^\alpha_n(\vec{k})}{N_n(\vec{k})}\,\psi_n(\vec{k},\vec{r})\,, \tag{2}$$

where

$$|N_n(\vec{k})|^2 = \int_{\text{unit cell}} |\psi_n(\vec{k},\vec{r})|^2\, d^3r\,. \tag{3}$$

The expansion coefficients C^α_n are determined from solution of the secular equations

$$\sum_{n'} [E_n(\vec{k})\delta_{nn'} + \Delta_{nn'}(\vec{k})]C^\alpha_{n'}(\vec{k}) = E_\alpha(\vec{k})C^\alpha_n(\vec{k})\,, \tag{4}$$

where the muffin-tin correction matrix elements are given by

$$\Delta_{nn'}(\vec{k}) \equiv \frac{1}{N_n(\vec{k})N_{n'}(\vec{k})} \int_{\text{unit cell}} \psi^*_n(\vec{k},\vec{r}) \times [V(\vec{r}) - V_{\text{MT}}(\vec{r})] \times \psi_{n'}(\vec{k},\vec{r})\, d^3r\,, \tag{5}$$

the integrand being nonzero only in the interstitial region of the unit cell. Since the crystal potential $V(\vec{r})$ and its muffin-tin counterpart $V_{\text{MT}}(\vec{r})$ have the full symmetry of the crystal, $\Delta_{nn'}(\vec{k})$ and the secular equation (4) are block diagonal according to the irreducible representations of the group of the wave vector $\vec{k}$. The numerical evaluation of the muffin-tin correction matrix element (5) was accomplished by choosing an integration grid in the interstitial region based on a midpoint algorithm in the two dimensions parallel to the graphite layers and Gaussian quadrature in the third dimension.[26] The total integration grid included 297 points within the irreducible sector ($\frac{1}{24}$) of the unit cell. For evaluation of matrix elements between wave functions of symmetry lower than D_{6h}, the grid was extended as needed, by applying symmetry operations not included in the group of the wave vector to the grid points of the irreducible sector. The muffin-tin wave functions were evaluated as described in the Appendix. In order to achieve accurate results for all bands near and below the Fermi level, the muffin-tin basis set $\{\psi_n(\vec{k},\vec{r})\}$ for each $\vec{k}$ and irreducible representation was taken to span the energies from the lowest valence band to approximately 1.2 Ry above E_F.

The numerical error introduced in evaluating the muffin-tin correction matrix elements $\Delta_{nn'}(\vec{k})$ and by basis-set truncation is approximately ± 0.01 Ry for bands near E_F. The error is somewhat higher for bands appreciably above E_F due to basis-set truncation and also somewhat higher for the low-energy σ bands due to inadequacy of the integration grid for treating these highly localized wave functions.

IV. RESULTS OF BAND-STRUCTURE CALCULATION

A. Band structure of LiC_6

The labeling of the symmetry points and directions in a hexagonal unit cell has been taken to be that of Herring[10] in his study of hexagonal-close-packed structures, having symmetry D^4_{6h} as shown in Fig. 1(c). The state labels for the D^1_{6h} structure of LiC_6 can be taken to be the same as for D^4_{6h} in the $k_z = 0$ plane. However, in the $k_z = \pi/c$ plane the D^4_{6h} labels no longer pertain to D^1_{6h}. We therefore chose to label the $k_z = \pi/c$ states with the same subscripts and superscripts as for the corresponding $k_z = 0$ states, but using the letters appropriate for the location in the Brillouin zone.[10] Since the center of symmetry was chosen at a Li site, carbon π and σ states change labels as k_z changes from $k_z = 0$ to $k_z = \pi/c$.

The most complete calculations were carried out using the ionic potential $Li^+C_6^-$. The results are given in Fig. 3 along the directions M-Σ-Γ-T-K (the $k_z = 0$ plane), Γ-Δ-A (the c axis), and L-R-A-S-H (the $k_z = \pi/c$ plane). Here the π bands of carbon are represented by dashed lines, while the σ bands are represented by full lines. Because of the choice of the center of symmetry, C π states are labeled $\Sigma_3, \Sigma_2, T_3, T_2$, etc., in the $k_z = 0$ plane, while they are labeled R_1, R_4, S_1, S_4, etc., in the $k_z = \pi/c$ plane. On the basis of this band structure, it will be established that LiC_6 has occupied valence bands which are essentially those of graphite with an A-A layer stacking. This result indicates that LiC_6 is a π-band metal. The lowest band having appreciable Li $2s$ character has its minimum at the Γ point (Γ_1), at least 1.7 eV above the Fermi level. This metal band hybridzes with C σ bands in the $k_z = 0$ plane and with C π bands in the $k_z = \pi/c$ plane; it is clearly dis-

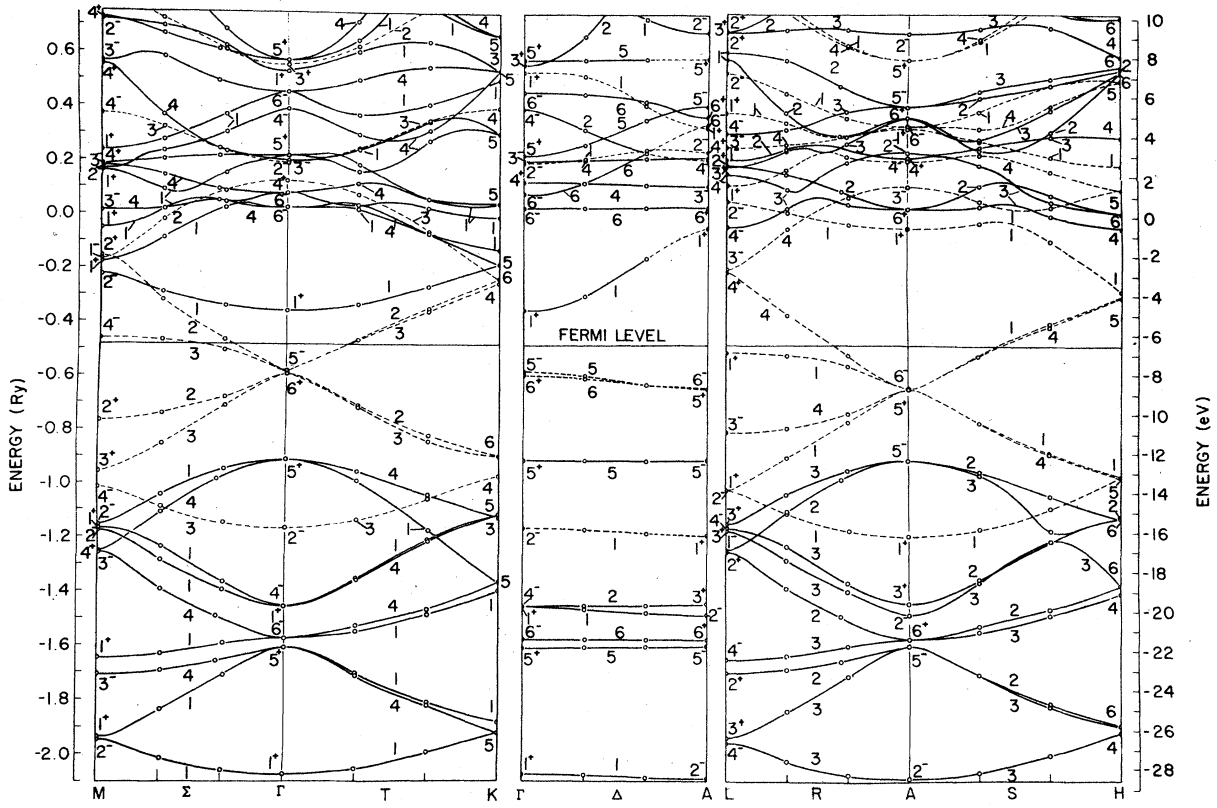

FIG. 3. Accurate band structure of LiC_6 based on ionic crystal potential $Li^+C_6^-$. Carbon π bands are represented by dashed lines; σ bands are represented by full lines. Dispersion shown along M-Σ-Γ-T-K ($k_z = 0$ plane), Γ-Δ-A, and L-R-A-S-H ($k_z = \pi/c$ plane).

tinguished from the graphite bands by its large dispersion along the c axis. Apart from this gross picture, the Li 2s states hybridize to some extent with low-lying graphite bands, particularly with a bonding π band. This latter point will be discussed more fully in paper II.[9]

B. Comparison with bands of graphite

In order to compare the band structure of LiC_6 with that of graphite, it is convenient to transform the graphite bands into the Brillouin zone of LiC_6. First consider the dispersion in the two dimensions parallel to a graphite layer. In these dimensions, the Brillouin zone of LiC_6 is one-third the area of the Brillouin zone of graphite, the K point for two-dimensional graphite mapping into the Γ point for the LiC_6 structure, and the M point for two-dimensional graphite mapping into the M point for the LiC_6 structure. Figure 4 shows the π bands of two-dimensional graphite, taken from the calculation of Painter and Ellis,[18] "folded" into the corresponding Brillouin zone of LiC_6. For contrast, Fig. 4 also contains a similar construction for the KC_8 structure, which will be discussed briefly in Sec. V.

The Fermi level of two-dimensional graphite occurs at the K point of the graphite Brillouin zone where the two π bands come together. In the LiC_6 Brillouin zone, these two π bands near the Fermi level of graphite are translated into four bands centered at Γ point in the $k_z = 0$ plane and at the A point in the $k_z = \pi/c$ plane. These four Fermi-level bands are found to be weakly bonding or antibonding in nature. In addition, there is a low-lying bonding π band and a high-lying antibonding π band, making a total of six π bands from the original graphite structure. The bonding and antibonding attributes of the π bands will be discussed more fully in paper II. Comparing the dispersion of the folded graphite bands shown in the central panel of Fig. 4 with that of the corresponding bands of LiC_6 shown in the two side panels of Fig. 3 reveals their striking similarity. The magnitudes of the band gaps at the Brillouin-zone boundaries indicate the strength of the Li perturbation. It will be shown in Paper II that the Li band hybridizes to an appreciable extent with the

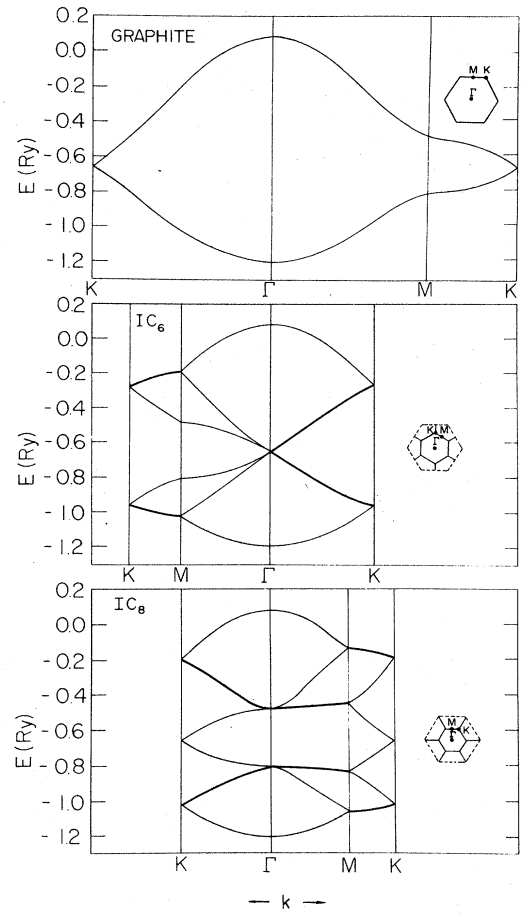

FIG. 4. π bands of two-dimensional graphite, adapted from the calculation of Painter and Ellis (Ref. 18); shown in the layer Brillouin zone of graphite (top), IC_6 (middle), and IC_8 (bottom), where I stands for intercalant. Insets show the relationships of two-dimensional Brillouin zones parallel to graphite layers. Degenerate bands are indicated with a thickened line.

lowest (bonding) π band of graphite. This interaction results in band gaps at M (M_3^+-M_4^-; 0.06 Ry) and at K (K_6-K_4; 0.07 Ry). In fact, these gaps are induced by an indirect interaction of Li $2s$ states with the C π states, the direct interaction being zero for symmetry reasons in the $k_z = 0$ plane. In the $k_z = \pi/c$ plane, the corresponding band gaps are negligible, presumably because the Li $2s$ states have much higher energy than at $k_z = 0$, which reduces the effective interaction. Further evidence of the lack of Li hybridization for $k_z = \pi/c$ states below E_F is shown by the degeneracy (within the accuracy of the calculation) of the S_1 and S_4 bands.[27] The first appreciable band gap for $k_z = \pi/c$ C π states occurs at H (H_1-H_5; 0.02 Ry), 0.2 Ry above E_F. Comparison of the occupied C σ bands of two-dimensional graphite[18] with those of LiC_6 (Fig. 3) shows that these are affected by intercalation to a lesser degree than are the C π bands.

Dispersion of the graphite π bands parallel to the c axis is almost an order of magnitude smaller than the dispersion parallel to the graphite layers; dispersion of the σ bands along the c axis is even smaller, due to relatively weak carbon interlayer interactions. The same trend is found for the occupied bands of LiC_6 as shown in the central panel of Fig. 3. As shown in Sec. V the c-axis dispersion of the LiC_6 Fermi-level bands is roughly the same magnitude as of the corresponding dispersion is graphite due to the interaction of A-A stacked carbon atoms.

C. Effects of muffin-tin corrections

The muffin-tin approximation for LiC_6 is expected to be unreliable for the reasons mentioned in Sec. III. Not only do the muffin-tin spheres contain only 46% of the crystal volume, but also fluctuations in the interstitial potential with respect to the mean V_{MI} are 1 Ry or higher in some regions. To appreciate this point, the results of the muffin-tin calculation for the potential $Li^+C_6^-$ are graphed in Fig. 5. The drastic differences between the complete calculation and the muffin-tin results can be seen by comparing Figs. 3 and 5, respectively. To a large extent, these differences can be understood to result from the fact that the muffin-tin approximation overestimates the interlayer interactions. This overestimation has the effect of exaggerating the c-axis dispersion and exaggerating the hybridization between C σ and C π bands with each other[27] and with the metal bands. The cause of this overestimation is a systematic error introduced by replacing the interstitial potential with the constant V_{MI}, thereby underestimating the attractive potential in the C plane and overestimating it in the Li plane. For the $Li^+C_6^-$ model, the mean- interstitial potential has the value $V_{MI} = -1.23$ Ry. The interstitial potential in a Li plane achieves a value of -0.45 Ry (the maximum) directly between centers of "empty" C hexagons and takes a value of -0.67 Ry directly between two C atoms. In contrast, the maximum value of the intersitial potential in a C plane is -1.12 Ry, which occurs at the center of a C hexagon and achieves values as low as -4 Ry in small regions near a C–C bond. Thus the correction potential $[V(\vec{r}) - V_{MT}(\vec{r})]$ has substantial valleys centered on the C planes and barriers centered on the Li planes which systematically decrease the interlayer interactions predicted by the muffin-tin approximation. The most important error of the muffin-tin approxima-

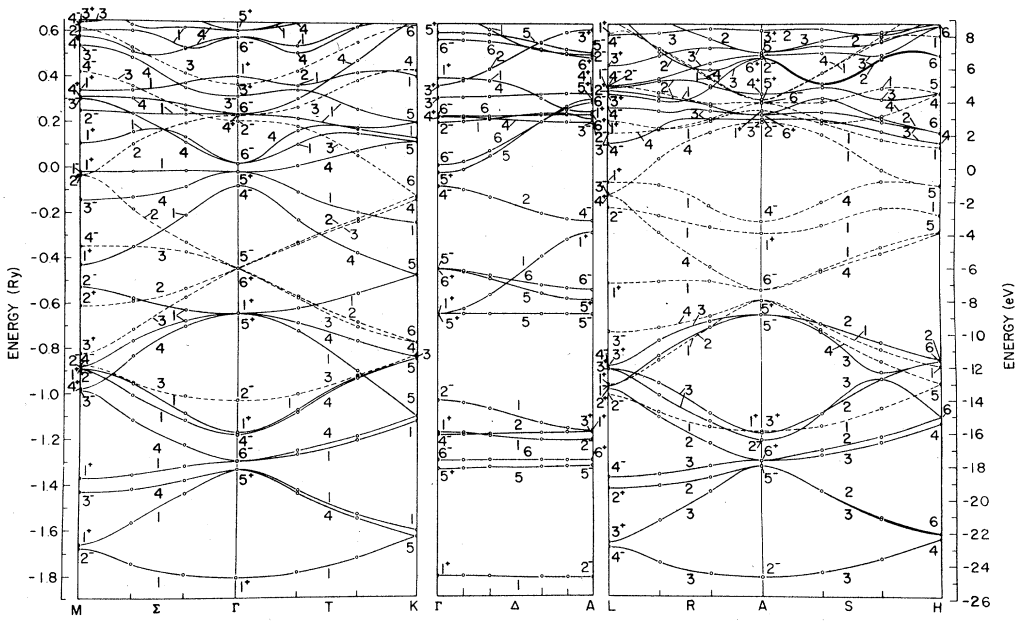

FIG. 5. Muffin-tin band structure of LiC_6 based on ionic crystal potential $Li^+C_6^-$. Carbon π bands are represented by dashed lines, C σ bands are represented by full lines, except along the Γ-Δ-A direction.

tion is its failure to predict the correct ordering of the bands near the Fermi level. The muffin-tin approximation predicts that the metal band lies below the Fermi level of graphite which is opposite the result established by the full calculations.

D. Effects of choice of crystal potential

Band-structure calculations along the high-symmetry line Γ-Δ-A were carried out for the crystal potential "LiC_6," generated from neutral-atom charge densities. These are compared with the corresponding results for the crystal potential "$Li^+C_6^-$," generated from ionic charge densities, in Fig. 6. The two band structures are qualitatively similar with some differences in detail. The important result is that for both approximations to the crystal potential, the metal band Γ_1^+-Δ_1-A_1^+ is predicted to lie above the Fermi level of graphite, and as we shall show in Sec. V, above the Fermi level of LiC_6. The gap between the bottom of the metal band (Γ_1) and the extremum of the graphite Fermi-level band (Γ_5^-) is 0.37 Ry for the LiC_6 potential model and 0.22 Ry for the $Li^+C_6^-$ potential model. The reduction of the gap for the $Li^+C_6^-$ potential model is consistent with the expectation that the ionic potential model has a larger relative strength toward the Li site than does the neutral potential model. One can reasonably argue that features of the band-structure results which depend upon the relative attractive potential contributions of the Li and C sites, as given by a self-consistent calculation, are bracketed by the two potential models $Li^+C_6^-$ and LiC_6. The $Li^+C_6^-$ model is expected to be closer to the self-consistent result than is the LiC_6 model, but is expected to slightly underestimate the screening of the Li^+ ion and therefore to overestimate its

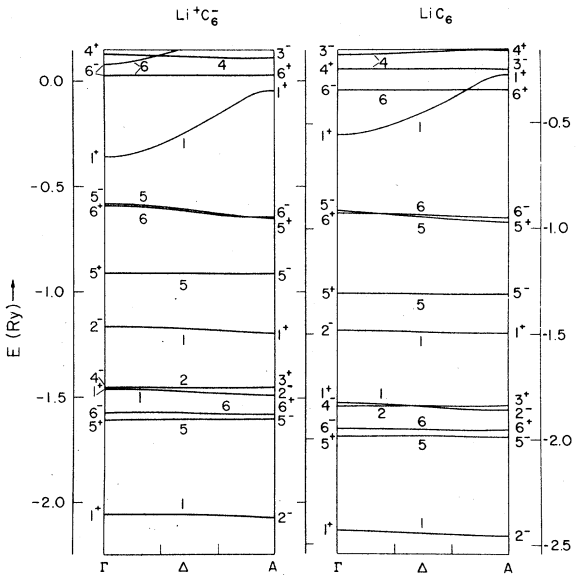

FIG. 6. Accurate band-structure calculations for LiC_6, comparing dispersion due to neutral potential "LiC_6" (right panel) with that due to ionic potential "$Li^+C_6^-$" (left panel) along the direction Γ-Δ-A.

TABLE II. LCAO parameters for Fermi-level bands of LiC_6 and graphite.

Interaction [a]	Value for LiC_6 (Ry)	Value for graphite (Ry)
$(C\ p_z\ C\ p_z\ \pi)_{1A}$	−0.185	±0.2 [b]
$(C\ p_z\ C\ p_z\ \pi)_{1B}$	−0.181	
$(C\ p_z\ C\ p_z\ \pi)_{2A}$	0.070	
$(C\ p_z\ C\ p_z\ \pi)_{2B}$	0.001	
$(C\ p_z\ C\ p_z\ \sigma)_z$	0.031	≈0.03 [c]
$(C\ p_z\ Li\ s)$	0.146	
$(C\ p_z\ Li\ p_{x,y})$	−0.159	
$(C\ p_z\ Li\ p_z)$	−0.147	
$E(C\ p_z)$	−0.545	
$E(Li\ s)$	−0.434	
$E(Li\ p_{x,y})$	−9	
$E(Li\ p_z)$	0.446	

[a] 1 and 2 denote nearest and next-nearest neighbors in a C plane; A denotes neighbors within a C hexagon "surrounding" Li site; B denotes neighbors within C hexagon "surrounding" empty site.

[b] Fit to bands of two-dimensional graphite (Ref. 18).

[c] Derived from Refs. 29 and 30.

relative attractive interaction. It follows that the results quoted in the present paper which are based on band-structure calculations using the $Li^+C_6^-$ model potential can be taken as the *lower limit* for energy separations between metal and graphite bands and as the *upper limit* for hybridization between metal and graphite states.

V. FERMI-LEVEL BANDS

A. LCAO parametrization of Fermi-level bands

In order to study the Fermi-level bands of LiC_6 in greater detail, a simple LCAO model[28] was fit to the accurate dispersion curves based on the $Li^+C_6^-$ potential (Fig. 3). Because the Fermi-level bands are weakly bonding and antibonding, they contain relatively little metal s-band character. It was therefore possible to fit these bands using only C π (p_z), Li s, Li p_{xy}, and Li p_z orbitals as basis functions and neglecting all Li-Li interactions. There were a total of 12 unknown parameters whose values are listed in Table II, where they are compared with LCAO parameters of graphite, derived from various sources.[18,29,30] It is evident that the LCAO parameters for the Fermi-level bands of LiC_6 are quite comparable to the corresponding parameters for graphite. The dispersion parallel to the graphite layers results mainly from the nearest-neighbor interaction with small second-neighbor contributions. The dispersion along the c direction can be explained by an interlayer C-C interaction. Its value is similar to the interlayer A-A carbon interaction is graphite[31] which is to be expected since the carbon layer spacings differ by only 10%. Li parameters of the LCAO model listed in Table I are obviously not realistic; this is presumably due to the neglect of Li-Li and Li-C σ interactions. The overall quality of the fit to the LiC_6 Fermi-level bands is good, the maximum error in the energy range −0.85 – −0.40 Ry being 0.01 Ry. Using the LCAO model as an interpolation formula, the density of states and Fermi surface parameters could be calculated.

B. Density of states near the Fermi level

The density-of-states histogram of LiC_6 is presented in Fig. 7. From the integrated density of states, the Fermi level for LiC_6 is located at E_F = −0.4815 Ry. At this energy there are two partly filled bands having C π characters, the lower containing 0.74 electrons, the upper containing 0.26 electrons. Since the minimum of the Li 2s band is located at −0.357 Ry, it is therefore established that the Li 2s band is completely empty and that the Fermi level lies within the π bands of graphite, as suggested by the early rigid-band theory.[8]

It is interesting to compare the density-of-states histogram for LiC_6 (Fig. 7) with that of graphite as calculated by Willis, Fitton, and Painter.[32] The density of states for graphite is distinguished

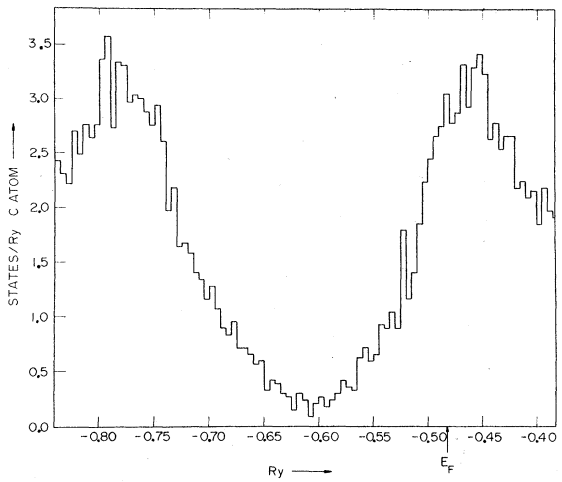

FIG. 7. Histogram of density of states Fermi-level bands of LiC_6 derived from LCAO model of $Li^+C_6^-$ band-structure results.

by a minimum due to the meeting of the bonding and antibonding π bands at its Brillouin-zone edge, flanked by maxima corresponding to saddle-point dispersion of these bands near the M point for two-dimensional graphite (see top panel of Fig. 4). These basic features are clearly evident in the density of states of LiC_6 shown in Fig. 7. According to a rigid model of intercalation, the Fermi level for first-stage intercalation compounds should be found near the M-point maxima in the density of states of graphite. The value of $N(E_F)$ for LiC_6 according to the rigid-band model using density-of-states results of Willis, Fitton, and Painter is comparable to the value calculated in the present work. The value of $N(E_F)$ for LiC_6 is found to be 0.24 states/(C-atom eV) (see Table III), in good agreement with the value of 0.21 $\pm$ 0.01 states/(C-atom eV) derived from the specific-heat measurements of Delhaes, Rouillon, Manceau, Guerard, and Herold,[33] although smaller than $N(E_F)$ derived from the Pauli susceptibility measured by the same authors. The larger value of the measured Pauli susceptibility over the calculated one-electron value is consistant with the enhancement expected from the exchange interactions of the C π electrons.

C. Fermi surface properties

The location of the Fermi level for LiC_6 derived from the integrated density of states is shown in relationship to the dispersion curves in Fig. 3. From this diagram, it is seen that the Fermi level is located at an energy below the lower band near $M_4^- - \Sigma_3$ but above it near $L_1^+ - R_1$, indicating that the lower-band Fermi surface cuts the Brillouin-zone boundary in each M-K-H-L plane. This feature of the band structure is a remnant of the saddle-point dispersion at the M point of the π bands of two-dimensional graphite. Both the upper- and lower-band Fermi surfaces cut the Brillouin-zone boundaries at $k_z = \pm\pi/c$. A perspective drawing of the Fermi surfaces is shown in Fig. 8 and cross sections of the Fermi surfaces in the $k_z = 0$ and $k_z = \pi/c$ planes are given in Fig. 9. For comparison, cross sections of the Fermi surfaces derived from the rigid-band model of LiC_6, based on the two-dimensional graphite band structure of Painter and Ellis,[18] is shown in Fig. 10. The calculated LiC_6 Fermi surface cross sections in the $k_z = 0$ plane are very similar although smaller in comparison to those predicted by the rigid-band model; the cross sections in the $k_z = \pi/c$ are distorted due to contact with the Brillouin-zone boundary. Once the Fermi surface has been determined, various parameters of experimental interest can be calculated. In addition to $N(E_F)$ discussed in Sec. V B above, plasma frequencies, and optical masses, as well as cyclotron frequencies and masses have been calculated for LiC_6.

The dielectric tensor of any material having a

TABLE III. Fermi-level density of states, plasma frequencies, and optical masses.

	Lower band	Upper band	Total
Conduction electrons per unit cell	0.74	0.26	1
Fermi-level DOS, $N(E_F)$ [states/(C-atom eV)]	0.19	0.04	0.24
ω_p^a (eV)	5.2	4.1	6.7
ω_p^c (eV)	1.9	0.9	2.2
m_{opt}^a/m_e	0.6	0.4	
m_{opt}^a/m_e	4.6	6.9	

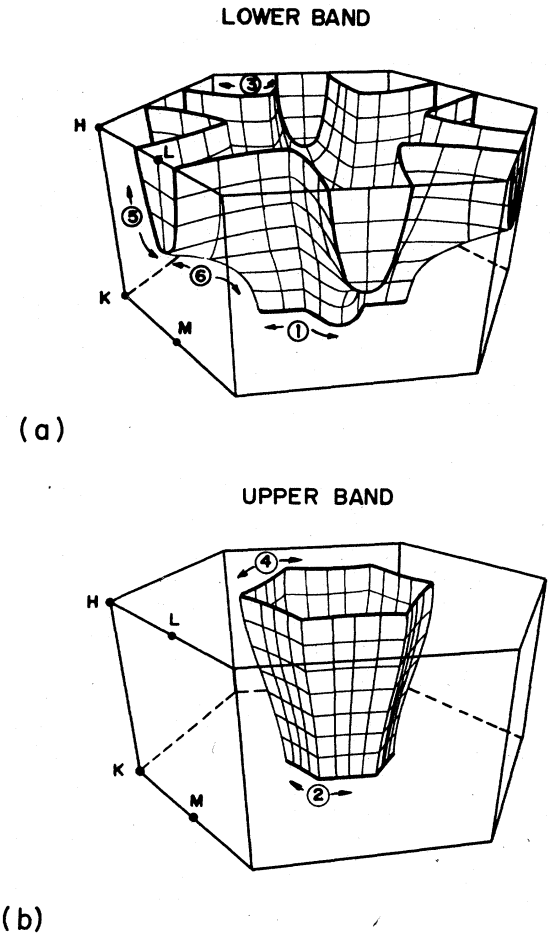

FIG. 8. Perspective drawings of the lower (a) and upper (b) band Fermi surfaces of LiC_6 based on calculation using $Li^+C_6^-$ potential and LCAO interpolation. Surfaces are given in $\frac{1}{2}$ of Brillouin zone between $k_z = 0$ and $k_z = \pi/c$ planes.

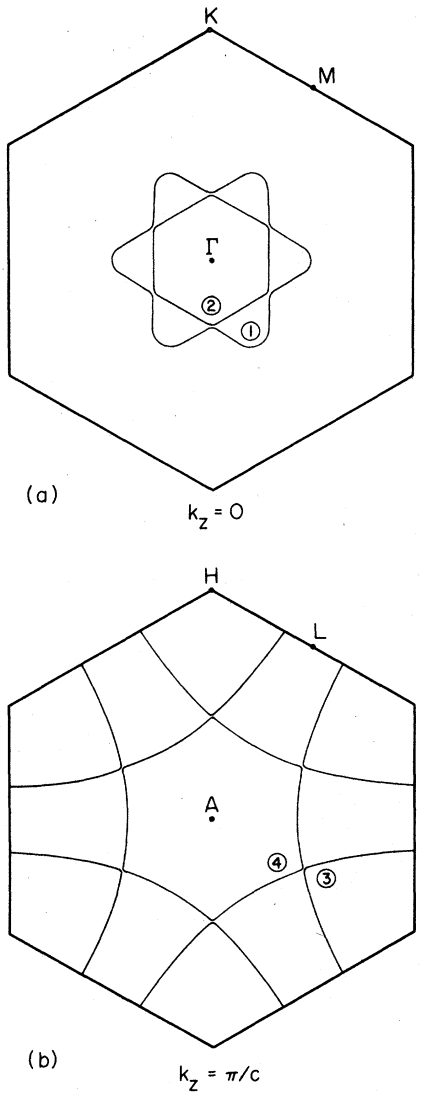

FIG. 9. Cross sections of Fermi surfaces of LiC_6 in $k_z = 0$ (a) and $k_z = \pi/c$ (b) planes based on calculation using $Li^+C_6^-$ potential and LCAO interpolation.

partly filled conduction band can generally be written as a sum of the form

$$\epsilon^{ij} = \delta_{ij} + \epsilon^{ij}_{\text{intraband}} + \epsilon^{ij}_{\text{interband}}, \tag{6}$$

where i,j refer to crystal axes. For carriers of infinite lifetime the intraband contribution to the dielectric tensor takes the form

$$\epsilon^{ij}_{\text{intraband}} = \frac{1}{\omega^2} \sum_\alpha (\omega_p^2)^{ij}_\alpha , \tag{7}$$

where the plasma frequency for the αth carrier is given by the Fermi surface (FS) integral[34]

$$(\omega_p^2)^{ij}_\alpha = \frac{4\pi e^2}{\hbar^2} \frac{2}{(2\pi)^3} \int_{\text{FS}} dS_{\vec{k}} \frac{1}{|\nabla E_\alpha(\vec{k})|} \times \frac{\partial E_\alpha(\vec{k})}{\partial k_i} \frac{\partial E_\alpha(k)}{\partial k_j} . \tag{8}$$

Alternatively, intraband optical results can be expressed in terms of the optical mass tensor[35] which is related to the plasma frequency according to

$$(\omega_p^2)^{ij}_\alpha = 4\pi e^2 n_\alpha (m^{-1}_{\text{opt}})^{ij}_\alpha , \tag{9}$$

where n_α is the number of electrons in band α per unit volume.

In many intercalated graphite compounds, the experimental visible and near-ultraviolet reflectivity spectrum is dominated by a reflectivity edge at a few eV.[1,36,37] This can be explained by plasma oscillations of the form of Eqs. (7)–(9)[38] plus a relatively large ($\gg 1$) and structureless background dielectric tensor arising from interband transi-

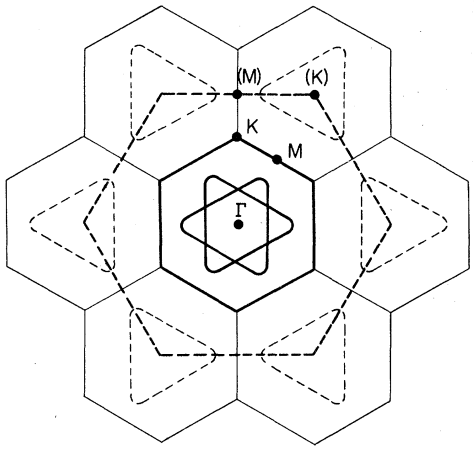

FIG. 10. Cross section of the Fermi surfaces of the two-dimensional rigid-band model of LiC_6 derived from band structure of two-dimensional graphite from calculation by Painter and Ellis (Ref. 18). Dashed lines denote Brillouin zone and Fermi surface in two-dimensional graphite structure.

tions at energies higher than the photon energies.[36,37] In LiC_6 the reflectivity is slightly complicated by the presence of low-energy interband transitions predicted from the present band-structure results and suggested by the experimental data.[37] From the band-structure results shown in Fig. 3, it can be seen that photons polarized parallel to the graphite planes can induced low-energy transitions near the Fermi level between the two carrier bands which are nearly degenerate along the T $(T_3 \rightarrow T_2)$, $S(S_1 \rightarrow S_4)$,[27] and intermediate directions.

An uniaxial crystal has two independent components of the plasma and optical mass tensors which can be denoted with superscripts a and c for polarizations in the x-y plane and along the z axis, respectively,

$$(\omega_p^a)_\alpha \equiv \{\tfrac{1}{2}[(\omega_p^2)_\alpha^{xx} + (\omega_p^2)_\alpha^{yy}]\}^{1/2}, \qquad (\omega_p^c)_\alpha \equiv [(\omega_p^2)_\alpha^{zz}]^{1/2}. \tag{10}$$

These have been evaluated for LiC_6 according to Eqs. (8) and (9) and the results are listed in Table III. The contributions from the two carriers are similar, although the anisotropy of the lower band is substantially less than that of the upper band due to its contact with Brillouin-zone boundaries parallel to the c axis. The reflectivity data of LiC_6 for photon polarizations parallel to the graphite planes[37] is consistent with the results listed in Table III. The anisotropy of the optical mass of the combined carriers is calculated to be

$$(\omega_p^2)^a_{\text{total}} / (\omega_p^2)^c_{\text{total}} \equiv m^c_{\text{opt}}/m^a_{\text{opt}} \approx 10 .$$

This anisotropy is smaller than the value of 11 for the corresponding anisotropy for KC_8 derived from polarized reflectance data.[36]

In order to further quantify the anisotropy of the Fermi surfaces of LiC_6, de Haas–van Alphen frequencies $F(\hat{H})$ and masses $m(\hat{H})$ have been evaluated from the Fermi surface line integrals:[39]

$$F(\hat{H}) = \frac{c\hbar}{2\pi e}\,\frac{1}{2}\int_0^{2\pi} k_\perp^2\, d\phi \tag{11}$$

and

$$\frac{m(\hat{H})}{m_e} = \frac{\hbar^2}{2\pi}\int_0^{2\pi} \frac{k_\perp\, d\phi}{|\hat{k}_\perp \cdot \nabla E_\alpha(\vec{k})|}, \tag{12}$$

respectively. Here $\vec{k}_\perp$ denotes the component of the Fermi wave vector perpendicular to the magnetic field whose magnitude $k_\perp$ depends upon an aximuthal angle ϕ. From Figs. 8 and 9, it is evident that the Fermi surfaces of LiC_6 have a total of six closed extremal orbits, indicated by the numbers. The de Haas–van Alphen frequencies and masses for these orbits are listed in Table IV. In general, the two orbits for the upper band (2 and 4) have lower frequency and smaller mass than the corresponding orbits of the lower band (1 and 3). There are two orbits for the lower band which would be observed with magnetic fields perpendicular to the c axis (orbits 5 and 6). Of these, only orbit 6 samples a significant amount of the c axis dispersion, resulting in a relatively large mass. Unfortunately, it is doubtful that all of the de Haas–van Alphen oscillations can be observed experimentally, not only because of the relatively poor quality of available graphite,[1] but also because of magnetic breakdown which could occur along the T, S, and intermediate directions, where the two carrier bands become nearly degenerate.[27]

TABLE IV. De Haas–van Alphen frequencies and masses.

	Band	Orbit Plane	Orbit Center	Type	F (10^8 G)	m/m_e
1	Lower	$k_z = 0$	Γ	Electron	0.40	0.98
2	Upper	$k_z = 0$	Γ	Electron	0.21	0.32
3	Lower	$k_z = \pi/c$	H	Hole	0.54	0.64
4	Upper	$k_z = \pi/c$	A	Electron	0.48	0.47
5	Lower	$k_x = \frac{2\pi}{3a}$	L	Electron	0.20	0.71
6	Lower	$k_y = 0$	M	Hole	0.55	2.13

TABLE V. Some predicted optical transition for LiC_6.

Transition [a]	Photon polarization [b]	$h\nu$ (Ry)	Comment [c]
	Allowed critical-point transitions		
$M_2^+ \rightarrow M_4^-$ $(\pi-\pi)$	$\vec{E} \parallel \hat{y}$	0.31	g (0.34 Ry)
$M_2^+ \rightarrow M_1^-$ $(\pi-\pi)$	$\vec{E} \parallel \hat{x}$	0.60	f
$M_3^+ \rightarrow M_4^-$ $(\pi-\pi)$	$\vec{E} \parallel \hat{x}$	0.50	f
$L_1^+ \rightarrow L_3^-$ $(\pi-\pi)$	$\vec{E} \parallel \hat{y}$	0.30	f
$L_1^+ \rightarrow L_4^-$ $(\pi-\sigma)$	$\vec{E} \parallel \hat{z}$	0.39	m
$L_1^+ \rightarrow L_2^-$ $(\pi-M)$	$\vec{E} \parallel \hat{x}$	0.57	m
$L_3^- \rightarrow L_4^+$ $(\pi-\pi)$	$\vec{E} \parallel \hat{x}$	0.60	f
$\Gamma_6^+ \rightarrow \Gamma_6^-$ $(\pi-\sigma)$	$\vec{E} \parallel \hat{z}$	0.62	f (~0.7)
$A_6^- \rightarrow A_6^+$ $(\pi-\sigma)$	$\vec{E} \parallel \hat{z}$	0.67	f
$\Gamma_2^- \rightarrow \Gamma_1^+$ $(\pi-M)$	$\vec{E} \parallel \hat{z}$	0.81	m
$\Gamma_5^+ \rightarrow \Gamma_6^-$ $(\sigma-\sigma)$	$\vec{E} \perp \hat{z}$	0.94	g (~0.9)
$A_5^- \rightarrow A_6^+$ $(\sigma-\sigma)$	$\vec{E} \perp \hat{z}$	0.95	g
	Noncritical-point transitions near Fermi level		
$T_3 \rightarrow T_2$, $S_1 \rightarrow S_4$ $(\pi-\pi)$	$\vec{E} \parallel \hat{x}$	$0 \leq h\nu \leq 0.02$	f
$\Sigma_3 \rightarrow \Sigma_2$, $R_1 \rightarrow R_4$ $(\pi-\pi)$	$\vec{E} \parallel \hat{y}$	$0.07 \leq h\nu \leq 0.30$	f
$\Sigma_3 \rightarrow \Sigma_1$, $T_3 \rightarrow T_1$ $(\pi-M)$	$\vec{E} \parallel \hat{z}$	$0.15 \leq h\nu \leq 0.22$	m

[a] π and σ denote primarily C bands, M denotes primarily Li band.

[b] Coordinates labeled according to Fig. 1(b); $\vec{E} \parallel \hat{x}$ denotes six equivalent polarizations as does $\vec{E} \parallel \hat{y}$.

[c] g denotes transition allowed in graphite value in parentheses calculated for two-dimensional graphite (Ref. 18); f denotes transition introduced by Brillouin-zone folding; m denotes transition to metallike band.

VI. DISCUSSION AND CONCLUSIONS

There have been relatively few experimental results for LiC_6 published to datae. This is primarily due to the past difficulty of synthesis.[5] However, a new synthesis technique developed by Zanini, Basu, and Fischer[37] promises to make high-quality c-face crystals available for experiment in the near future. As discussed above, the present results are in good agreement with the specific-heat measurement of $N(E_F)$,[33] and are consistent with visible and near-ultraviolet reflectance measurements.[37] In Paper II, we will make qualitative comparison of the present results with NMR and Raman measurements. In general, we find that the present band-structure results are consistent with all currently available experimental information for LiC_6; however, further experimental information is needed to carry out rigorous comparison of theory and experiment. For example, an extended optical study would be very helpful for testing the details of the present band-structure results. Table V lists the important critical point transitions for $h\nu \lesssim 0.6$ Ry and some important noncritical point transitions for low-energy transitions involving the Fermi-level bands. Some higher-energy transitions are also listed in order to compare with similar transitions in graphite. The most well-documented transition in graphite occurs at 4.6 eV,[18] and is associated with the saddle-point dispersion of the π bands at the M point of two-dimensional graphite. The corresponding transition in LiC_6, $M_2^+ \rightarrow M_4^-$, is calculated to occur at slightly lower photon energies (~4.2 eV). We expect this M-point transition to have less intensity in LiC_6 than it does in graphite because roughly only $\frac{1}{2}$ as many final states are above the Fermi level. Some intensity will be gained, however, by a $L_1^+ \rightarrow L_3^-$ transition at nearly the same photon energy. Painter and Ellis[18] predict the energy difference between the Fermi level of graphite and the bottom of the σ band to be ~0.7 Ry. Corresponding transitions in LiC_6 are $\Gamma_6^+ \rightarrow \Gamma_6^-$ and $A_6^- \rightarrow A_6^+$ having predicted energies 0.62–0.67 Ry. This correspondance is reasonable in view of the fact that there is hybridization of the

upper σ bands with Li 2s states. Similarly the separation of σ bands in graphite is calculated to be 0.9 Ry,[18] in correspondance with the 0.94–0.95 Ry transitions $\Gamma_5^+ \rightarrow \Gamma_6^-$ and $A_5^- \rightarrow A_6^+$ predicted for LiC_6. We predict the separation between the π band and Li band minima, $\Gamma_2^- \rightarrow \Gamma_1^+$, to be 0.81 Ry. In addition to these critical-point features, the optical spectrum of LiC_6 is expected to have some absorption at low energy due to transitions involving the Fermi-level bands, as listed on the bottom of Table V. Transitions induced by photon polarizations $\vec{E} \perp \hat{z}$ are introduced by the folding of the graphite bands into the Brillouin zone of LiC_6. Transitions induced by photon polarizations $\vec{E} \parallel \hat{z}$ involve the Li band as the final state. In order to estimate the strength of these transitions, the interband contribution to the dielectric tensor (6) should be calculated.

An important property of graphite intercalation compounds is their electrical conductivity. We have made no attempt to calculate the conductivity for LiC_6, although some qualitative information is provided by the Fermi surface parameters listed in Tables III and IV. In particular, if one could neglect the anisotropy in the scattering lifetime τ, the ratio of the conductivity parallel to the graphite layers σ_a to that parallel to the c axis σ_c would be given by the ratio of the optical masses $\sigma_a/\sigma_c \approx m^c_{\rm opt}/m^a_{\rm opt} \simeq 10$, as discussed in Sec. V. Because of the neglect of the anisotropy of τ, this value should not be taken seriously except to point out that the anisotropy in the conductivity of LiC_6 is expected to be substantially reduced from that of graphite for which $\sigma_a/\sigma_c \simeq 10^3$.[1] A contributing factor to the reduction of anisotropy is the A-A carbon-layer stacking of LiC_6. The c-axis dispersion of the Fermi-level bands of LiC_6 is determined by the interaction of neighboring layer (α-α) C π orbitals separated by 3.7 Å.[5] However, in graphite, due to the A-B carbon-layer stacking, a significant fraction of the carriers (e.g., the majority electrons) are in a band of mainly E_3 character,[30] whose c-axis dispersion is determined by the interactions of next-nearest-layer (β-β) C π orbitals, separated by 6.7 Å.[30] Since even the largest first-stage-donor intercalation compound CsC_8, has an α-α carbon-layer spacing of 5.9 Å[1] which is smaller than the β-β carbon-layer spacing of graphite, one might expect the conductivity anisotropy of graphite to be reduced by all donor intercalates, as is seen experimentally.[1] For the MC_8 compounds it has been suggested[1,7,36,40] that another contributing factor to the reduction of conductivity anisotropy is the presence of some "three-dimensional carriers" which are formed from the hybridization of the Fermi-level graphite π bands with the metal band,[7] unlike the situation we have found for LiC_6. If it were not for the presence of three-dimensional carriers and differences in scattering processes, we would expect the conductivity anisotropy for LiC_6 to be lower than that of the MC_8 compounds because of its smaller C-layer spacing and because of its Fermi surface cutting the Brillouin-zone boundary.

It is interesting to compare the present band structure of LiC_6 with the band structure of KC_8 determined by an extended Hückel calculation by Inoshita, Nakao, and Kamimura.[7] The two-dimensional Brillouin zone of KC_8 is $\frac{1}{4}$ the area of that of graphite, the M point of graphite mapping into the Γ point of KC_8, resulting in the folded π band structure shown in bottom panel of Fig. 4. The important K-point structure of the graphite bands is found at the K point in KC_8, instead of at the Γ point as in LiC_6. If the two-dimensional rigid-band model were appropriate for KC_8 one would expect the Fermi surface to be centered at the K point as shown in Fig. 11 in contrast to that centered at the Γ point for LiC_6 shown in Fig. 10. The two-dimensional rigid-band model predicts a single-sheeted Fermi surface for the KC_8, structure, whereas the LiC_6 structure has a double-sheeted Fermi surface. The band-structure results of Inoshita, Nakao, and Kamimura[7] show some resemblance to the rigid-band model of Figs. 4 and 11, although deviations are introduced by the staggered K-layer stacking of KC_8 and by hybridization of the metal bands with the graphite bands

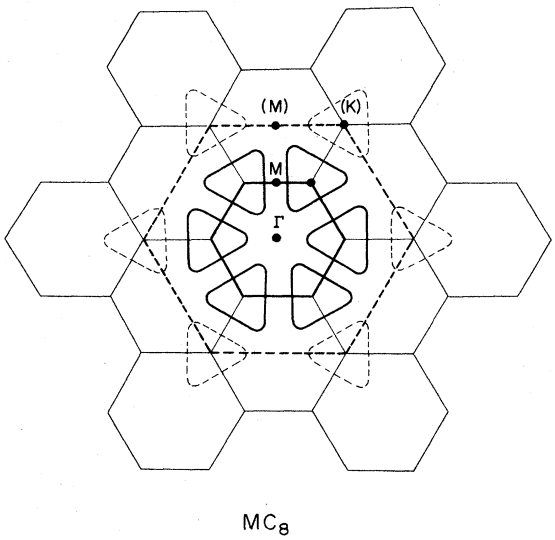

FIG. 11. Cross section of the Fermi surfaces of the two-dimensional rigid-band model of I C_8 derived from the band structure of two-dimensional graphite from calculation by Painter and Ellis (Ref. 18). Dashed lines denote Brillouin zone and Fermi surface in two-dimensional graphite structure.

near the Fermi level. No significant hybridization is predicted between the K 4*s* states and the low-lying bonding π bands of graphite; however, this result could be due to the choice of basis set used in the calculation.[7] An interesting feature of calculated KC_8 band structure[7] is the relatively small *c*-axis dispersion of the metal bands. An unoccupied metal band is found to have a *c*-axis bandwidth 2–3 times smaller than the corresponding metal *c*-axis bandwidth found for LiC_6. This suggests that the metal bands in KC_8 have some two-dimensional character. Energetic reasons for the possible qualitative differences between KC_8 and LiC_6 are discussed in Paper II. It will be interesting to see whether or not the extended Hückel predictions[6,7] for KC_8 are corroborated by more accurate band-structure calculations.

In conclusion, the results of our detailed band-structure calculations indicate that the two-dimensional rigid-band model of intercalation provides a good zeroth-order approximation to the *Fermi-level properties* of LiC_6. Important modifications of the two-dimensional rigid-band predictions are, however, caused by the "band folding" due to the periodic perturbation of the intercalate layers and caused by the interlayer interactions of the graphite layers in LiC_6, resulting in *c*-axis dispersion. The qualitative, but not necessarily quantitative, success of the rigid-band model in explaining the Fermi-level properties of LiC_6 can be attributed to the fact that the metal band does not appreciably hybridize with the weakly bonding and antibonding Fermi-level bands of graphite and to the fact that the bottom of the metal band lies at least 1.7 eV above the Fermi level of LiC_6. Properties of LiC_6 which depend upon states appreciably above or below E_F, such as optical transitions or total charge distribution, are not well approximated by the rigid-band model, as will be discussed further in Paper II.[9]

APPENDIX: EVALUATION OF THE MUFFIN-TIN WAVE FUNCTIONS

The muffin-tin wave function $\psi_n(\vec{k},\vec{r})$, corresponding to the solution of Eq. (1) at energy $E_n(\vec{k})$ with scattered-wave amplitudes $W^{\sigma}_{lm}(\vec{k},E_n)$ can be generally evaluated as a sum of two terms

$$\psi_n(\vec{k},\vec{r}) = \psi(\text{scatt}) + \psi(\text{MT sphere}). \tag{A1}$$

The sum of coherently scattered wave diverging from each atom is given by

$$\psi(\text{scatt}) = \sum_s{}' \sum_{\sigma l m} e^{i\vec{k}\cdot(\vec{\tau}_\sigma+\vec{t}_s)} W^{\sigma}_{lm}\, i h_l(\kappa|\vec{r}-\vec{\tau}_\sigma-\vec{t}_s|)\, Y_{lm}((\vec{r}-\vec{\tau}_\sigma-\vec{t}_s)/|\vec{r}-\vec{\tau}_\sigma-\vec{t}_s|), \tag{A2}$$

and can be conveniently evaluated by an Ewald expansion[15,25]

$$\begin{aligned}\psi(\text{scatt}) = {}& \frac{4\pi}{\Omega\kappa}\sum_{\vec{G}} e^{i(\vec{k}+\vec{G})\cdot\vec{r}}\,\frac{\exp\{[\kappa^2-(\vec{k}+\vec{G})^2]/\eta\}}{(\vec{k}+\vec{G})^2-\kappa^2}\sum_{\substack{\sigma l m\\(l\le L)}} i^{-l}\, e^{-i\vec{G}\cdot\vec{\tau}_\sigma}\left(\frac{|\vec{k}+\vec{G}|}{\kappa}\right)^{l} Y_{lm}\left(\frac{\vec{k}+\vec{G}}{|\vec{k}+\vec{G}|}\right) W^{\sigma}_{lm}\\ &+\frac{1}{\sqrt{4\pi}}\sum_{s\sigma}{}'\sum_{\substack{lm\\(l\le L)}} e^{i\vec{k}\cdot(\vec{\tau}_\sigma+\vec{t}_s)}\int_0^{\kappa^2/\eta} du\, u^{-3/2-l}\exp\left(\frac{u-\kappa^2|\vec{r}-\vec{\tau}_\sigma-\vec{t}_s|^2}{4u}\right)\left(\frac{\kappa|\vec{r}-\vec{\tau}_\sigma-\vec{t}_s|}{2}\right)^{l} Y_{lm}\left(\frac{\vec{r}-\vec{\tau}_\sigma-\vec{t}_s}{|\vec{r}-\vec{\tau}_\sigma-\vec{t}_s|}\right)\\ &+\sqrt{\eta}\,\frac{1}{2\pi\kappa}\sum_{\lambda=0}^{\infty}\left[\left(\frac{\kappa^2}{\eta}\right)^{\lambda}\frac{1}{\lambda!}\,\frac{1}{(2\lambda-1)}\right]\sum_{s\sigma}\delta_{\vec{r},\vec{\tau}_\sigma+\vec{t}_s}\, e^{i\vec{k}\cdot(\vec{\tau}_\sigma+\vec{t}_s)} W^{\sigma}_{00}.\end{aligned} \tag{A3}$$

Here $\vec{\tau}_\sigma$ locates the atoms in the unit cell, $\vec{t}_s$ is a lattice tranlation vector, h_l is a spherical Hankel function of the first kind, κ denotes the scalar wave vector

$$\kappa \equiv [(2m/\hbar^2)(E_n - V_{\text{MI}})]^{1/2}, \tag{A4}$$

Ω denotes the volume of the unit cell, $\vec{G}$ is a reciprocal-lattice vector, and η is the Ewald parameter.[15] ψ(scatt) represents the wave function in the interstitial region. Inside each muffin-tin sphere, the wave function deviates from the scattered wave for Eqs. (A2) and (A3) by an amount

$$\psi(\text{MT sphere}) = \sum_{\sigma s} e^{i\vec{k}\cdot(\vec{\tau}_\sigma+\vec{t}_s)} \sum_{\substack{lm\\(l\le L)}} W^{\sigma}_{lm}\,[R^{n}_{lm}(\vec{r}-\vec{\tau}_\sigma-\vec{t}_s) - f^{n}_{\sigma l m}(\vec{r}-\vec{\tau}_\sigma-\vec{t}_s)], \tag{A5}$$

where

$$f^{n}_{\sigma l m}(\vec{x}) \equiv \sum_{l'm'} j_{l'}(\kappa x) Y_{l'm'}(\hat{x}) K^{\sigma-1}_{l'm',lm} - (1-\delta_{\vec{r},\vec{\tau}_\sigma+\vec{t}_s}) n_l(\kappa x) Y_{lm}(\hat{x}), \tag{A6}$$

is a component of the expansion of ψ(scatt) about the muffin-tin center. $R^n_{\sigma l m}(\vec{x})$ of Eq. (A5) is the regular solution to the radial Schrödinger equation appropriate for the crystal potential expanded in spherical harmonics about the site σ, satisfying the boundary and normalization condition

$$R^n_{\sigma l m}(\vec{x}) = f^n_{\sigma l m}(\vec{x}) \quad \text{for } x \geq r^{\sigma}_{\mathrm{MT}} . \tag{A7}$$

Thus ψ(MT sphere) is nonzero only inside a muffin-tin sphere. In order to avoid divergence, Eqs. (A2), (A3), and (A6) make use of a primed summation over atomic sites which means that the term $\vec{\tau} = \vec{\tau}_\sigma + \vec{t}_s$ is to be excluded while $\delta_{\vec{\tau},\vec{\tau}_\sigma+\vec{t}_s}$ denotes the Kronecker δ function for the same term. The convenience of the above representation of the muffin-tin wave function is that even for such a highly anisotropic material as LiC_6, the partial-wave sums in Eqs. (A6) are rapidly converging ($l \leq L$). By proper choice of the Ewald parameter, the lattice and reciprocal-lattice sums of Eq. (A3) can also be made to be rapidly converging.

Note added in proof. N. Kambe, M. S. Dresselhaus, G. Dresselhaus, S. Basu, A. R. McGhie, and J. E. Fischer [Mater. Sci. Eng. (to be published)] have recently determined, on the basis of transmission electron diffraction, that LiC_6 has an $\alpha\beta\gamma$ stacking at $T \leq 220$°K. Their results at room temperature are consistent with either an $\alpha\beta$ stacking or a disordered stacking. We expect the present band-structure results, based on the D^1_{6h} structure, to be only weakly modified by the structural differences.

ACKNOWLEDGMENTS

The present work was facilitated by the technical assistance of Jerry Feldman, especially in generating the three-dimensional drawings of the Fermi surfaces. We would also like to acknowledge stimulating discussions with M. Zanini, P. Soven, and J. Fischer. Our special thanks are due to the staffs of the Moore School and David Rittenhouse Laboratory computer facilities. Financial support for this work was given partly by the National Science Foundation through the University of Pennsylvania Materials Research Laboratory, Grant No. DMR-76-00678 and partly by the Pennsylvania Science and Engineering Foundation, Grant No. PSE F-365.

[1]Some recent review articles are F. R. Gamble and T. H. Geballe, *Treatise on Solid State Chemistry*, edited by N. B. Hannay (Plenum, New York, 1976), Vol. 3. p. 89; L. B. Ebert, Annu. Rev. Mater. Sci. 6, 181 (1976); J. E. Fischer, *Physics and Chemistry of Materials with Layered Structures*, edited by F. Lévy (Reidel, Dordrecht, Holland, 1977) Vol. 5; A. Hérold, *ibid*; M. S. Dresselhaus, *ibid*.

[2]*Proceedings of the Franco-American Conference on Intercalation Componds of Graphite*, edited by F. L. Vogel and A. Hérold, Mater. Sci. Eng. 31, Dec. 1977. Included in this reference is a preliminary report of the present work, p. 195.

[3]J. E. Fischer and T. E. Thompson, Phys. Today 30, 18 (1977); 31, 36 (1978).

[4]R. Juza and V. Wehle, Naturwissenschaften 52, 560 (1965).

[5]D. Guerard and A. Herold, Carbon 13, 337 (1975); D. Guerard, Thèse doctorat des sciences (Nancy, France, 1974) (unpublished).

[6]R. Swanson, Ph.D. thesis (Stanford University, 1969) (unpublished).

[7]T. Inoshita, K. Nakao, and H. Kamimura, J. Phys. Soc. Jpn. 43, 1237 (1977).

[8]This idea is reviewed by M. C. Robert, M. Oberlin, and J. Mering [Chem. Phys. Carbon 10, 141 (1973)].

[9]N. A. W. Holzwarth, L. A. Girifalco, and S. Rabii, following paper, Phys. Rev. B 18, 5206 (1978).

[10]C. Herring, J. Franklin Inst. 233, 525 (1942).

[11]J. C. Slater, *The Self Consistent Field for Molecules and Solids* (McGraw-Hill, New York, 1974).

[12]C. A. Coulson, *Valence* (Oxford U. P., New York, 1953), p. 191ff.

[13]F. Herman and S. Skillman, *Atomic Structure Calculations*, (Prentice-Hall, Englewood Cliffs, N.J., 1963).

[14]This value is the simple mean of the α parameters of Li and C listed by K. Schwartz [Phys. Rev. B 5, 2466 (1972)].

[15]P. O. Ewald, Ann. Phys. (Leipz.) 49, 1 (1916).

[16]J. Korringa, Physica (Utr.) 13, 392 (1947); W. Kohn and N. Rostoker, Phys. Rev. 94, 1111 (1954).

[17]J. O. Dimmock, Solid State Phys. 26, 103 (1971); D. D. Koelling, Phys. Rev. 188, 1049 (1969).

[18]G. S. Painter and D. E. Ellis, Phys. Rev. B 1, 4747 (1970). These authors performed an LCAO-type calculation for graphite using a total of nine functions per C atom. A similar basis set for LiC_6 would require at least 63 basis functions per unit cell.

[19]H. Nagayoski, K. Nakao, and Y. Uemura, J. Phys. Soc. Jpn. 41, 2480 (1976).

[20]L. F. Mattheiss, Phys. Rev. B 13, 2433 (1976). For these materials of the rutile structure, 280 basis functions are required restricting calculations to $\vec{k}$ points of high symmetry.

[21]G. S. Painter, Phys. Rev. B 7, 3520 (1973).

[22]See, for example, P. Roman, *Advanced Quantum Theory* (Addison-Wesley, Reading, Mass., 1965), p. 488.

[23]W. John, G. Lehmann, and P. Ziesche, Phys. Status Solidi B 53, 287 (1972).

[24]B. Segall, J. Phys. Chem. Solids 8, 371 (1959); F. S. Ham and B. Segall, Phys. Rev. 124, 1786 (1961).

[25]K. Kamke, Z. Naturforsch. A 22, 322 (1967); 22, 422 (1967); 23, 1280 (1968).

[26]Because of the irregularity of integration region, it is difficult to use quadrature integration techniques for all three dimensions.

[27]The results of the accurate band-structure calculation shown in Fig. 3. indicate that the paired S_1 and S_4 bands in the $k_z = \pi/c$ plane have the opposite ordering of the corresponding T_3 and T_2 bands in the $k_z = 0$ plane, meaning that these two bands must cross for some k_z. This unphysical result is seen to be caused by the muffin-tin basis functions. In the muffin-tin calcualtion the "unphysical" ordering results from an overestimation of the interlayer interactions causing hybridization of the π bands with nearby σ bands for $0 < k_z < \pi/c$. The hybridization is essentially removed by the non-muffin-tin corrections, so that in the accurate calculation the energy separation between the two bands is 0.01 Ry, i.e., within the expected error of the calculation. The paired S_1 and S_4 bands must therefore be considered degenerate within the accuracy of the present calculation.

[28]J. C. Slater and G. F. Koster, Phys. Rev. 94, 1498 (1954).

[29]L. G. Johnson and G. Dresselhaus, Phys. Rev. B 7, 22 (1973).

[30]I. L. Spain, Chem. Phys. Carbon 8, 1 (1973); M. S. Dresselhaus and G. Dresselhaus, Phys. Rev. B 13, 4635 (1976); M. S. Dresselhaus, G. Dresselhaus, and J. E. Fischer, *ibid.* 15, 3180 (1977).

[31]It is interesting to note that the LCAO parameter for the C interlayer interaction which fits the bands of the LiC_6 potential (Fig. 6.) is approximately $\frac{2}{3}$ of that of the $Li^+C_6^-$ potential. This lends support to suggestion, based on the arguments presented in Sec. IV D, that the results of the band-structure calculation based on the $Li^+C_6^-$ potential give the *upper limit* of the c-axis dispersion.

[32]R. F. Willis, B. Fitton, and G. S. Painter, Phys. Rev. B 9, 1926 (1974).

[33]P. Delhaes, J. C. Rouillon, J. P. Manceau, D. Guerard, and A. Herold, J. Phys. (Paris) 37, L-127 (1976).

[34]N. F. Mott and H. Jones, *The Theory of the Properties of Metals and Alloys* (Dover, New York, 1958), p. 96ff; A. H. Wilson, Proc. R. Soc. A 151, 274 (1935).

[35]M. H. Cohen, Philos. Mag. 3, 732 (1958).

[36]M. Zanini and J. E. Fischer, Ref. 2, p. 169.

[37]M. Zanini, S. Basu, and J. E. Fischer, Carbon 16, 211 (1978).

[38]The effects of finite lifetime of the carriers is usually taken into account in fitting the data (see Ref. 36).

[39]A. V. Gold, in *Solid State Physics, Electrons in Metals*, edited by J. F. Cochran and R. R. Haering (Gordon and Breach, New York, 1968), Vol. 1, p. 39.

[40]T. Kondow, U. Mizutani, and T. B. Massalski, in Ref. 2, p. 267.